Phase transformation of a vortex beam in a liquid-based inferior mirage

OPEN ACCESS
IOP Publishing
Journal of Optics
J. Opt. **22** (2020) 125605 (8pp)
https://doi.org/10.1088/2040-8986/abc6fb

Phase transformation of a vortex beam in a liquid-based inferior mirage

Claire M Cisowski[1,2] **and Ricardo R B Correia**[2]

[1] Dept. of Physics and Astronomy, SUPA, University of Glasgow, Glasgow G12 8QQ, United Kingdom
[2] Instituto de Física, Universidade Federal do Rio Grande do Sul, Av. Bento Gonçalves, Porto Alegre 91501-970, Brazil

E-mail: clairemarie.cisowski@glasgow.ac.uk

Received 17 August 2020, revised 12 October 2020
Accepted for publication 2 November 2020
Published 23 November 2020

Abstract

We study how a liquid-based inferior mirage, obtained by layering distilled water and ethanol, transforms the phase structure of a light beam possessing a helical wave front. An inferior mirage amounts for one total internal reflection, which effectively reverses the handedness of the wave front. We show that this transformation is accompanied by smooth unidirectional astigmatic changes and variations of the non-canonical strength of the phase singularity nested in the beam. A skew in the beam intensity distribution is observed where the phase singularity is inverted and allows the direct measurement of the topological charge of the beam. Freely propagating, partially inverted beams possessing spatially varying orbital fluxes can be obtained at the exit plane of the solution by adjusting the incidence conditions of the beam. This work lays the foundations for phase engineering of light beams in liquid-based optical mirages.

Supplementary material for this article is available online

Keywords: OAM, vortex beam, mirage effect

(Some figures may appear in colour only in the online journal)

1. Introduction

Optical mirages are well known effects appreciated in nature for centuries. At the origin of these effects is a vertical gradient of refractive index (VGRIN) modifying both the amplitude and phase of the optical beam propagating through it [1]. While changes in the beam intensity structure such as distortions and deflections have been extensively studied [2], phase transformations have mostly been overlooked. However, a mirage amounts for a total internal reflection (mirror inversion), upon which the whole phase structure of the beam is disrupted and angular momentum is reversed. Unlike total internal reflection occurring at a sharp interface between two media of different refractive index, in a VGRIN, total internal reflection occurs progressively, through several layers of different refractive index. This allows a deconstruction and appreciation of the dynamics of the phase transformation in optical mirages.

In this paper, we examine the phase effects of an optical mirage for the first time. This experiment is realised by layering liquids of different densities and refractive indexes (distilled water and ethanol). We are particularly interested in the transformation of beams with a helical phase structure, known as helical beams. Indeed, these beams carry orbital angular momentum (OAM), a particularity that has been exploited for multiple applications [3]. Mirror inversion is known to reverse the handedness of helical beams [4], meaning that a beam with OAM $+\ell\hbar$ per photon transforms into a beam carrying $-\ell\hbar$ per photon, where ℓ is the topological charge of the beam. Therefore, we expect optical mirages to bring new insight into the dynamics of handedness reversal.

Understanding how helical beams transform upon propagation is paramount, especially in the domain of communication

[5–7]. VGRIN describing a cylindrical lens or a locally compressed optical fibre have been shown to affect the phase structure of helical beams [8, 9]. These VGRIN progressively break the cylindrical symmetry of the helical beam in one direction, much like a liquid-based VGRIN. Hence, we expect to witness similar effects on phase transformation, inclusive of some major differences as we explore the total internal reflection and the fact that a liquid-based VGRIN is significantly more complex. Notably, a liquid-VGRIN does not possess an axial symmetry and evolves according to diffusion. The first section of this paper presents the realization and characterization of the liquid-based VGRIN and describes how to obtain a quasi-stationary inferior mirage. Then, the phase transformation of a helical beam propagating through the solution is examined numerically and experimentally. Intensity changes accompanying the phase transformation are also examined.

2. Realization and characterization of a liquid-based VGRIN

In the laboratory, VGRIN have mainly been realized using either heated plates or liquid superposition [2]. We rely on the latter technique, which is easy to implement and minimizes edge effects. We superpose a layer of distilled water (refractive index, $n_{H_2O} = 1.3429$ [10]) and ethanol (refractive index, $n_{C_2H_6O} = 1.3725$ [11]). First, we fill a cylindrical glass cell of inner diameter 26 mm and length 200 mm, enclosed with two quartz windows, with distilled water until the water level reaches a height of 15 mm. Ethanol ($>99.9\,\%$) is then added until the cell is filled while exercising caution to minimize the mixing of the two liquids. Ethanol has a lower density than distilled water, establishing a VGRIN through the solution. Considering that the refractive index does not vary along the horizontal direction, the refractive index of the solution as a function of the height above the initial interface of the liquids y can be expressed as [12]:

$$n(y) = n_{H_2O} + (n_{C_2H_6O} - n_{H_2O})\left(\frac{a'\mu(y) + b'\mu(y)^2 + c'\mu(y)^2}{a' + b' + c'}\right) \quad (1)$$

where a', b', c' are constants. For clarity, we may write:

$$n(y) = n_{H_2O} + a \cdot \mu(y) + b \cdot \mu(y)^2 + c \cdot \mu(y)^3 \quad (2)$$

where $a = 7.972 \times 10^{-2}$, $b = -3.706 \times 10^{-2}$, $c = -1.381 \times 10^{-2}$. In equations (1) and (2), $\mu(y)$ is the mass fraction of ethanol as function of liquid height, which reads [13, 14]:

$$\mu(y) = (1 + \frac{2}{\sqrt{\pi}} \int_0^{y/d} e^{-t^2 \mathrm{d}t})/2 \quad (3)$$

where d is the diffusion length of this quasi-stationary distribution, which evolves according to $d^2 = 4Dt$ where t is measured in hours. $D = 1.22 \times 10^{-5}$ cm^2 s^{-1} is the inter-diffusion constant of the two liquids [15]. Figure 1 shows the refractive index profile as function of liquid height, fifteen minutes and four hours after the cell is filled with both liquids.

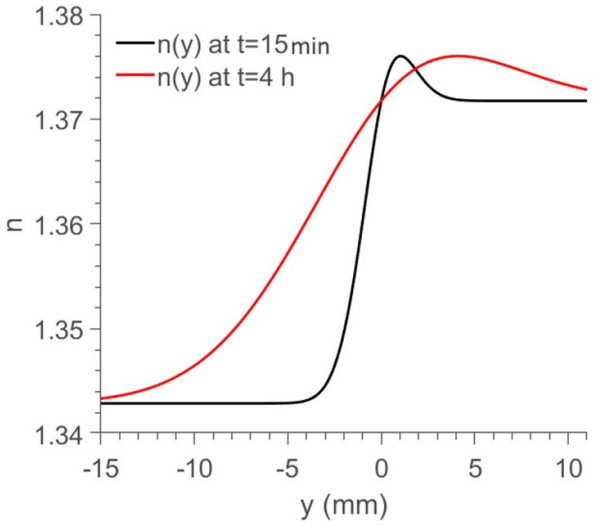

Figure 1. Refractive index of the solution as function of liquid height (calculated with respect to the liquid interface at $t = 0$), 15 min and 4 h after the cell has been filled.

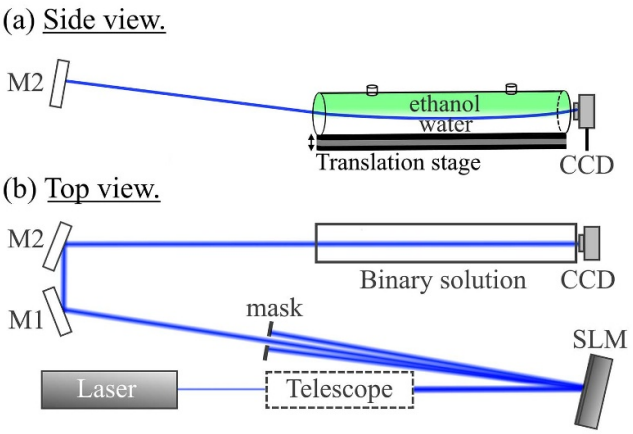

Figure 2. Experimental setup includes two planar mirrors (M1, M2), a spatial light modulator (SLM) and a charged-couple device (CCD) camera. (a) Side view showing the beam propagation after M2. (b) Top view showing the entire setup.

The liquid-based VGRIN is dynamic and more complex than that describing a cylindrical lens or a compressed fibre. Diffusion decreases the steepness of the VGRIN distribution over time and a peak in the refractive index, of higher value than the refractive index of the pure components alone is observed. This peak is due to a contraction of the water-ethanol mixture [16].

The liquid-based VGRIN is probed by a helical beam. Figure 2 illustrates our experimental setup.

The output of a Fabry–Perot laser diode source of wavelength $\lambda = 405$ nm is collimated through a telescope to obtain a beam with a waist radius of 450 μm. A reflective phase spatial light modulator (SLM), displaying a fork diffraction hologram, imparts an helical phase structure to the first-order diffracted beam. This beam is spatially selected by blocking

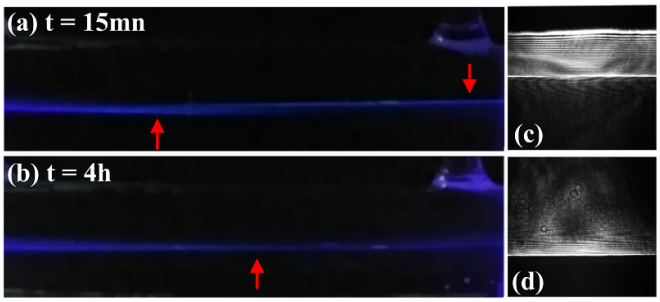

Figure 3. Experimental trajectories (a), (b) and intensity distributions (c), (d) of a beam of topological charge $\ell = +1$ propagating through a water-ethanol column for an incidence height $y_{\text{in}} = 4$ mm and for an incidence angle $\theta_{in} = 1.5^{\circ}$ at $t = 15$ min and $t = 4$ h are shown. Deflection points are indicated by red arrows. (c), (d) Recorded by the CCD camera near the exit plane of the water–ethanol column.

other diffracted order with an opaque mask. The angle of incidence of the light beam upon the solution is fixed to $\theta_{\text{in}} = 1.5^{\circ}$ using a pair of mirrors (M1, M2). The water-ethanol column is placed on a micrometric vertical stage to allow the incidence height of the beam upon the solution y_{in} to be varied. A CCD camera of resolution 1296×964 and pixel size 3.75 μm is juxtaposed to the exit plane of the column to record the intensity distribution of the beam exiting the cell.

We examine the trajectory of a helical beam propagating through the solution at $t = 15$ min and $t = 4$ h, corresponding to the two VGRIN profiles shown on figure 1. To do so, we fix the incident height of the beam to be $y_{\text{in}} = 4$ mm (4 mm above the water-ethanol interface defined at $t = 0$). The incident beam has a topological charge $\ell = +1$, which amounts for the number of 2π phase windings around a phase singularity. The trajectories are shown on figures 3(a) and (b) and are recorded by a camera oriented perpendicularly to the water–ethanol column main axis. Figures 3(c) and (d) show the intensity distribution of the beam at the exit plane of the solution and are recorded by the CCD camera shown in figure 2.

At $t = 15$ min, two inflection points are visible on figure 3(a), whereas a single inflection point is observed at $t = 4$ h (figure 3(b)). These trajectories give rise to distinct intensity distributions at the exit of the water–ethanol column, as shown on figure 3(c) for $t = 15$ min and figure 3(d) for $t = 4$ h. Figure 3(d) corresponds to an inferior mirage where the beam was reflected once in the upward direction, causing a single mirror inversion event. This introduces astigmatism along the vertical direction. In practice, mirror inversion can easily be verified by blocking the upper part of the beam prior to entering the water-ethanol column and observing whether the upper or lower part of the beam exiting the solution is obstructed. Figure 3(c) corresponds to a Fata Morgana, which is a complex form of a mirage comprising several inverted and non-inverted images. Here, the beam has experienced two consecutive reflections, the second reflection is caused by the peak in the refractive index profile as shown in figure 1. Thus, depending on the VGRIN profile, more than a single beam inversions can take place within our solution.

For clarity, we study the transformation of a helical light beam experiencing a single mirror inversion, i.e. as an inferior mirage. Thus, in the subsequent sections, we consider the VGRIN formed 4 h after the cell has been filled in 20 min periods, which is considered quasi-stationary ($< 5\%$ variations in the refractive index profile) over 20 min periods.

3. Phase dynamics in a liquid-based inferior mirage

In order to experimentally study how a helical beam transforms upon mirror inversion, we vary the incidence height of the light beam y_{in} such that mirror inversion takes place near the exit plane of the solution where it can be recorded. The incidence angle of the beam is kept constant (1.5°).

The experimental intensity distributions of an incident helical light beam of topological charge $\ell = +1$ exiting the solution for different incidence heights are shown as gray scale images on the right panel of figure 4. The respective numerical intensity distributions at the exit plane (in false colours on the right panel of figure 4) as well as the numerical trajectory of the beam propagating through the column (left panel of figure 4) are plotted. The numerical analysis is realized with a semi-vectorial beam propagation method implemented by the software BeamLab. The VGRIN profile is also provided on the right side of each trajectory plot for a determinate height range.

For an incidence height of the light beam above the interface of $y_{in} = 8.3$ mm, the beam experiences a region of negative VGRIN and follows a U-shaped trajectory as shown in figure 4(a). In this case, the beam exiting the solution (figure 4(f)) is not inverted. As the incidence height decreases, the beam encounters a region of positive VGRIN and gradually undergoes one mirror reflection (figures 4(b)–(e)). Figures 4(g)–(i) correspond to partially inverted beams and figure 4(j) shows a fully inverted beam.

We observe a small difference of vertical symmetry between an astigmatic non-inverted beam (figure 4(f)), where the main axis is tilted to the left, and an astigmatic fully inverted beam (figure 4(j)), where the main axis is tilted to the right, which is more perceptible in our numerical results. This indicates that the non-inverted and the inverted beam are of opposite topological charge [17]. This can be verified by determining the average orbital angular momentum of the beams using a tilted convex lens. The intensity distributions of a non-inverted and a fully inverted beam exiting the solution near the focal plane of a tilted convex lens are examined in figure 5 for incident beams of topological charge $\ell = +1, +2, +3$. The differences of axial symmetry between a fully non-inverted and a fully inverted beam indicate that the beams are of opposite handedness [18].

This confirms that mirror inversion reverses the handedness of the helical wave front, the handedness characterizing the phase increase around the phase singularity of the beam which can be clockwise or anti-clockwise. Handedness reversal is a well known phenomena routinely exploited in interferometric arrangements [19–21]. In practice, handedness reversal is

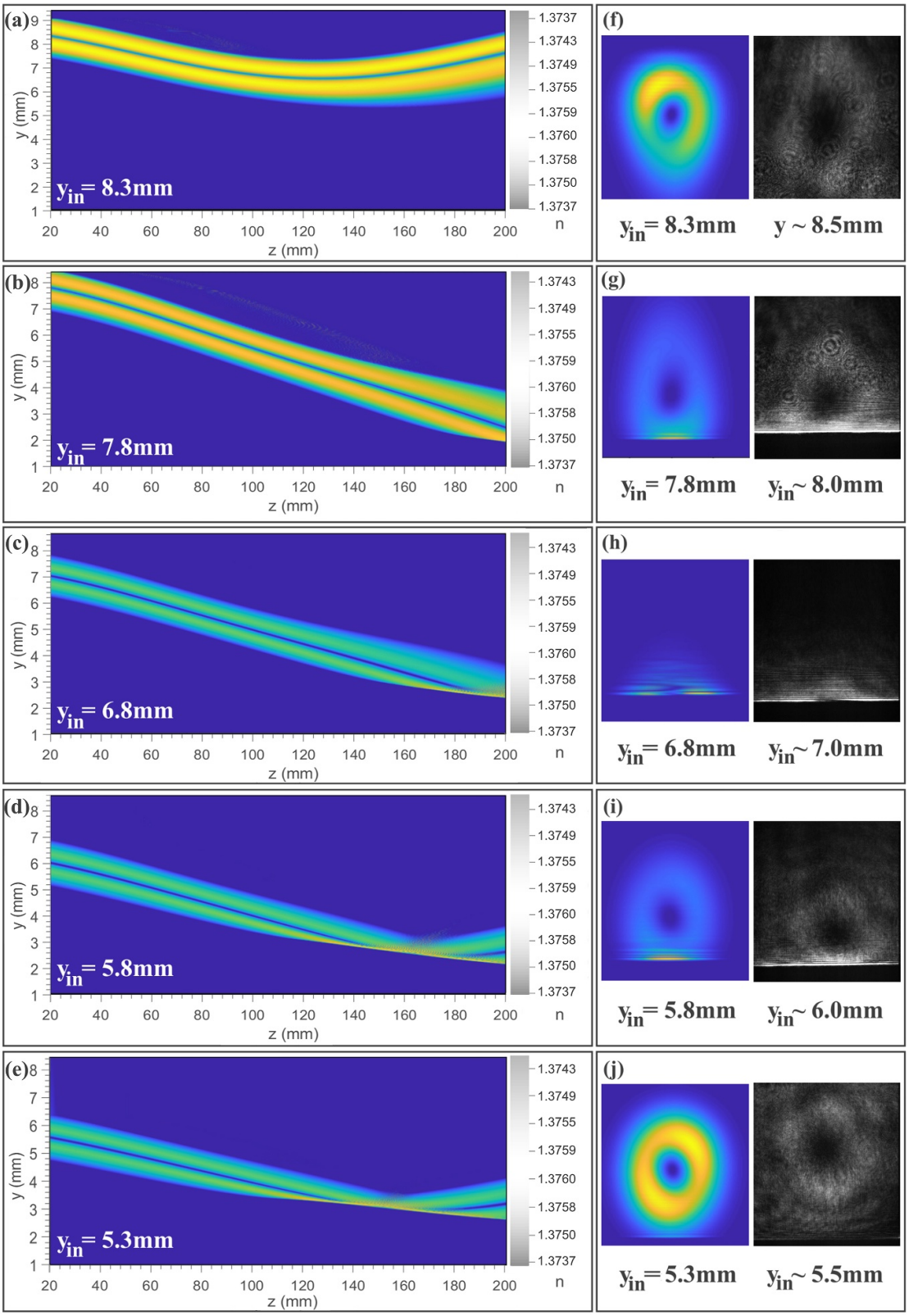

Figure 4. Numerical trajectory (left panel), and numerical and experimental intensity distributions at the exit plane of the binary solution (right panel) of a beam of topological charge $\ell = +1$ entering the solution with an incidence angle of 1.5° and for various incidence heights y_{in} (defined with respect to the water–ethanol interface at $t = 0$) is shown. The VGRIN profile is represented on the right side of the trajectory plots.

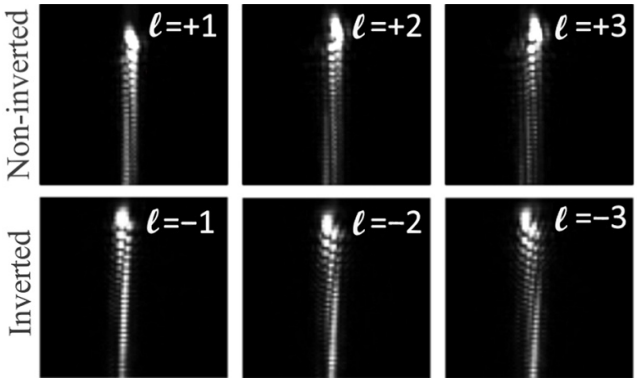

Figure 5. Intensity distributions near the focal plane of a tilted convex lens for helical light beams of topological charge $\ell = +1, +2, +3$, that have and have not experienced mirror inversion in the water-ethanol column. The number and orientation of the dark lines separating the chain of bright lobes indicate the beam topological charge, written on each image.

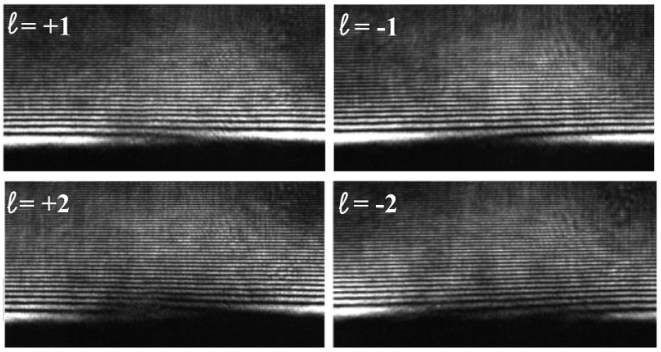

Figure 6. Intensity distributions at the exit plane of the solution, for incident beams of topological charge $\ell = +1, -1, +2, -2$, observed when the optical vortex core is being inverted (for $y_{in} =$ 6.8 mm and $\theta_{in} = 1.5°$) The fringes indicate self-interference between the inverted and non inverted parts of the beam.

often carried out by Dove prisms. In such a case, the phase transformation occurs abruptly upon total internal reflection at the glass–air interface [4]. In a VGRIN, this transformation occurs smoothly, through several layers of different refractive index, unraveling the dynamics of handedness reversal.

Figures 5(g)–(j) show that smooth, continuous, unidirectional astigmatic changes occur upon mirror inversion, i.e. as handedness reversal occurs. A screenshot of the video of this transformation showing how the intensity of the beam exiting the solution evolves as the incidence height of the beam upon the solution is lowered is given in appendix A (for the full video, please see the online supplementary material, available at (stacks.iop.org/JOPT/22/125605/mmedia)). These changes are similar to the ones reported near the focal plane of a cylindrical lens [8] or in a compressed fibre [9] upon handedness reversal except that for the present incidence conditions, the beam is asymmetrically focused along the vertical direction. Naturally, not all astigmatic changes caused by the VGRIN are related to handedness reversal. This is the case for $y_{in} =$ 8.3 mm, where the beam follows a U-shaped trajectory, exits the solution non-inverted and vertically stretched (figure 4(f)), conserving the topological charge. Similar astigmatic changes, unrelated to handedness reversal have recently been reported in a plasma density gradient [17].

Figure 4(h) shows the beam intensity distribution at a critical stage where the optical vortex, i.e. the phase singularity, undergoes mirror inversion. The experimental intensity distribution is magnified in figure 6, where the respective intensities distributions for incident beams of topological charge $\ell = +1, -1, +2, -2$ are also presented.

The helical beam is partially inverted at the exit plane of the solution. Both the inverted part and the non-inverted part of the beam appear superimposed. Fringes in the intensity distributions of figures 4 and 6 result from self-interference between the inverted and non-inverted parts of the beam. The fringe spacing varies according to the local wave vector vertical gradient at the exit plane of the water-ethanol column. This overlap can be used to determine the phase structure of the beam. A sharp skew in the beam intensity distribution, dependent on the topological charge of the incident beam, is visible where the optical vortex is being inverted. The same characteristic skew can be witnessed at the focal plane of a cylindrical lens [8].

The topological charge of the incident beam can thus be identified in a liquid-based mirage by lowering the incidence height of the beam upon the solution such that the self-interference of the beam can be recorded. This dispenses with the need of using a secondary reference beam, which is often susceptible to careful alignment.

When exiting the water-ethanol column, the beam no longer experiences the VGRIN and propagates freely. Consequently, for $y_{in} = 6.8$ mm, where only half of the incident beam is inverted when it reaches the end of the solution, the beam remains half inverted upon free propagation and undergoes non-uniform deformations along the vertical direction according to the vertical wave vector gradient at the column exit, which can be inferred from the trajectory plots of figure 4(c). The freely propagating, partially inverted beam will present spatially varying orbital angular momentum fluxes which correspond to a non-trivial phase front. This new type of beam is particularly interesting to study the relationship between the host beam and its vortex core, which can be isolated in the inverted or non-inverted part of the beam.

We further study the evolution of the phase structure of the incident beam upon mirror inversion using a numerical model. For this study, the incidence height and incidence angle upon the solution are fixed. The beam undergoes one mirror inversion within the solution, as shown in figure 7(a). The phase and the intensity distributions of the beam are plotted in several xy planes indicated by red lines in figure 7(a), selected to show crucial stages of the transformation. The angle of incidence is chosen to be small, $\theta_{in} = 0.3°$, to distinguish the phase variation around the optical singularity from the phase background which varies rapidly at larger angles. For incidence conditions $y_{in} = 4.0$ mm and $\theta_{in} = 0.3°$, this entails that the beam is symmetrically focused along the vertical direction.

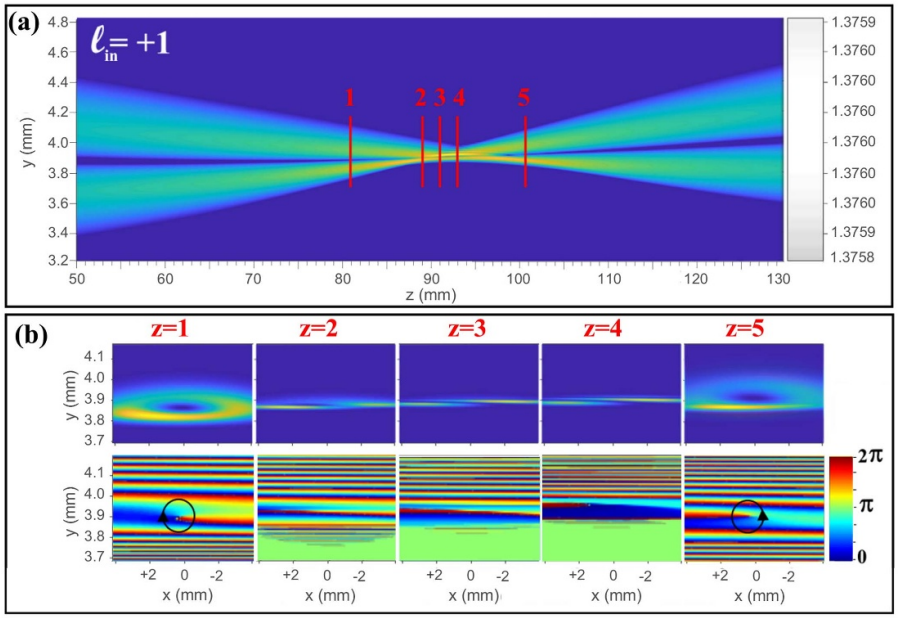

Figure 7. (a) Numerical trajectory of a beam of topological charge $\ell = +1$ propagating through the VGRIN for an incidence angle $\theta_{in} = 0.3^{\circ}$ and incidence height $y_{in} = 4.0$ mm. (b) Intensity and phase distribution in the planes indicated by red lines on (a), with $z_1 =$ 81mm, $z_2 = 89$ mm, $z_3 = 91$mm, $z_4 = 92$ mm and $z_5 = 101$ mm. The arrows indicate the direction of phase increase in a circuit around the optical singularity.

Figure 7(b) shows that the phase increment in a circuit around the optical vortex passes from being clockwise at z_1 to counter-clockwise at z_5, confirming once more that mirror inversion reverses the handedness of the beam.

The vortex nested within the incident beam is initially canonical, meaning that the phase increment with respect to the azimuthal angle around the vortex is linear [22]. In the vicinity of the critical plane, the phase evolution around the singularity is non-linear, as shown in figure 7(b) for z_1 and z_5. The video in appendix B shows the continuous evolution of the phase variation in the vicinity of the critical plane. The non-canonical strength of the optical vortex increases along with the astigmatism of the beam. In the critical plane (z_3), a phase discontinuity is observed, similar to the one found in Hermite-Gauss beams.

Additional numerical simulations showed us that helical beams hosting an high-order optical vortex see their optical vortex breaks down into unitary optical vortices prior to reaching the region of mirror inversion, which is due to their inherent instability [23]. Consequently, the transformation of a unitary order vortex shown in figure 7 applies to each one of the so-produced single vortex, namely, mirror inversion cause each vortex to undergo handedness reversal and, in the vicinity of the critical plane, each optical vortex becomes non-canonical. This entails that, for higher order helical beams, several phase discontinuities are observed in the critical plane, one for each unitary vortex core.

4. Conclusion

We have studied the phase transformation of a helical beam in a liquid-based inferior optical mirage. Upon mirror inversion, the handedness of the phase front is reversed. In a liquid-based VGRIN, this transformation is accompanied by continuous astigmatic changes along the vertical direction, which, for general conditions, describe asymmetric focusing along the vertical direction. These astigmatic changes are accompanied by continuous variations of the vortex non-canonical strength. In the critical plane where the optical vortex is inverted, the phase distribution is discontinuous. This translates into a skew in the intensity distribution, which allows to directly measure the topological charge of the incident beam. By adjusting the incidence conditions of the beam upon the VGRIN, a partially or a fully inverted beam can be obtained at the exit plane of the solution. This beam will propagate freely according to the vertical wave vector gradient at the exit plane and will present a non-trivial wavefront describing spatially varying orbital fluxes. This type of beam could be used to further investigate the relationship between the optical vortex core and its host beam. Partially inverted beams self-interfere at the exit plane of the solution, giving rise to characteristic fringes in the intensity distribution. Self-interference can potentially be used for wavefront sensing, which is useful not only for beams with helical wave front but also for general forms of phase-shaped light modes. In a liquid-based VGRIN, optically active elements can easily be added to the solution to interact with portions of the beam which are inverted—partially inverted and non-inverted—which opens perspectives for the study of light-matter interactions. In this study, we have studied mirror inversion within a VGRIN from a scalar perspective. In the near future, our group intends to explore the vectorial aspects of these phenomena.

Acknowledgments

This study was financed by the “Conselho Nacional de Desenvolvimento Científico e Tecnológico” and the “Coordenação

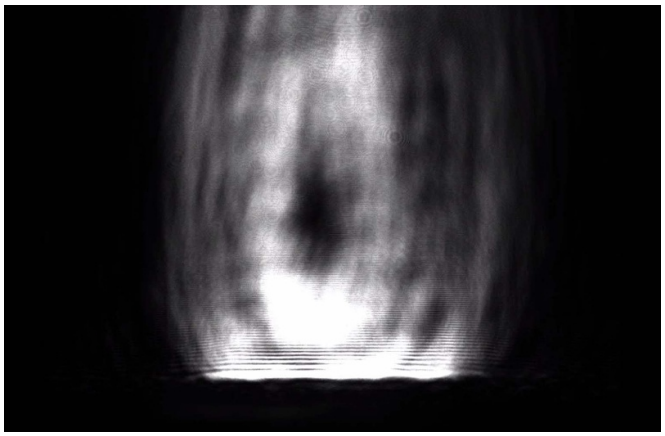

Figure A1. Formation of an inferior mirage.

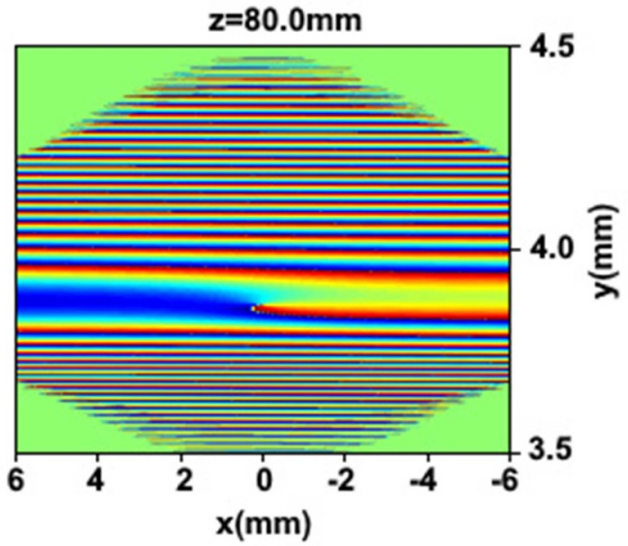

Figure B1. Computed phase distribution of an $\ell = +1$ helical light beam undergoing mirror inversion for an incidence height $y_{in} = 4.0$ mm, incidence angle $\theta_{in} = 0.3^{\circ}$, in the vicinity of the critical plane $z_3 = 91.0$ mm of figure 6.

de Aperfeiçoamento de Pessoal de Nível Superior—Brasil (CAPES)—Finance Code 001".

Appendix A

Figure A1 shows the experimental intensity distribution of a beam of topological charge $\ell = +1$ recorded by a CCD camera placed near the exit plane of the water-ethanol column. Mirror inversion occurs as the incidence height of the beam upon the solution is decreased, while maintaining a constant incidence angle ($\theta_{in} = 1.5^{\circ}$).

Appendix B

Figure B1 shows the phase evolution of a beam of topological charge $\ell = +1$ undergoing mirror inversion within the water-ethanol column. The phase is plotted in the transverse plane, for a propagation distance ranging from $z = 80$ mm to $z = 101$ mm. Handedness reversal entails continuous variations of the vortex canonical strength.

ORCID iD

Claire M Cisowski https://orcid.org/0000-0002-6422-5300

References

[1] Minnaert M 1993 *Light and Color in the Outdoors* (New York: Springer)
[2] Greenler R G 1987 Laboratory simulation of inferior and superior mirages *J. Opt. Soc. Am.* A **4** 589–90
[3] Padgett M, Courtial J and Allen L 2004 Light's orbital angular momentum *Phys. Today* **57** 35–40
[4] González N, Molina-Terriza G and Torres J P 2006 How a Dove prism transforms the orbital angular momentum of a light beam *Opt. Express* **14** 9093–102
[5] Padgett M J, Miatto F M, Lavery M P J, Zeilinger A and Boyd R W 2015 Divergence of an orbital-angular-momentum-carrying beam upon propagation *New J. Phys.* **17** 023011
[6] Lavery M P J, Peuntinger C, Günthner K, Banzer P, Elser D, Boyd R W, Padgett M J, Marquardt C and Leuchs G 2017 Free-space propagation of high-dimensional structured optical fields in an urban environment *Sci. Adv.* **3** 10
[7] Zhai Y, Fu S, Zhang J, Liu X, Zhou H and Gao C 2020 Turbulence aberration correction for vector vortex beams using deep neural networks on experimental data *Opt. Express* **28** 7515–27
[8] Molina-Terriza G, Recolons J, Torres J P, Torner L and Wright E M 2001 Observation of the dynamical inversion of the topological charge of an optical vortex *Phys. Rev. Lett.* **87** 023902
[9] Carpentier A, Michinel H, Salgueiro J, Doval S and Ferrando A 2006 Inversion of a guided optical vortex *J. Eur. Opt. Soc.* **1** 06031
[10] Daimon M and Masumura A 2007 Measurement of the refractive index of distilled water from the near-infrared region to the ultraviolet region *Appl. Opt.* **46** 3811–20
[11] Kozma I Z, Krok P and Riedle E 2005 Direct measurement of the group-velocity mismatch and derivation of the refractive-index dispersion for a variety of solvents in the ultraviolet *J. Opt. Soc. Am.* B **22** 1479–85
[12] Zhang T, Feng G, Song Z and Zhou S 2014 A single-element interferometer for measuring refractive index of transparent liquids *Opt. Commun.* **332** 14–17
[13] Mandelis A and Royce B S H 1984 Fundamental-mode laser-beam propagation in optically inhomogeneous electrochemical media with chemical species concentration gradients *Appl. Opt.* **23** 2892–901

[14] Rashidnia N and Balasubramaniam R 2002 Development of an interferometer for measurement of the diffusion coefficient of miscible liquids *Appl. Opt.* **41** 1337–42
[15] Hao L and Leaist D G 1996 Binary mutual diffusion coefficients of aqueous alcohols. Methanol to 1-heptanol *J. Chem. Eng. Data* **41** 210–3
[16] Lee I, Park K and Lee J 2013 Precision density and volume contraction measurements of ethanol–water binary mixtures using suspended micro-channel resonators *Sensors Actuators* A **194** 62–6
[17] Gong W, Shen B, Zhang X, Liangliang J and Zhang L 2019 Asymmetric optical vortex in plasma density gradient *Plasma Phys. Control. Fusion* **61** 125003
[18] Vaity P, Banerji J and Singh R P 2013 Measuring the topological charge of an optical vortex by using a tilted convex lens *Phys. Lett.* A **377** 1154–6
[19] de Oliveira A N, Walborn S P and Monken C H 2005 Implementing the Deutsch algorithm with polarization and transverse spatial modes *J. Opt. B: Quantum Semiclass. Opt.* **7** 288–92
[20] Leach J, Padgett M J, Barnett S M, Franke-Arnold S and Courtial J 2002 Measuring the orbital angular momentum of a single photon *Phys. Rev. Lett.* **88** 257901
[21] Zambrini R and Barnett S M 2006 Quasi-intrinsic angular momentum and the measurement of its spectrum *Phys. Rev. Lett.* **96** 113901
[22] Chen M and Roux F S 2008 Accelerating the annihilation of an optical vortex dipole in a gaussian beam *J. Opt. Soc. Am.* A **25** 1279–86
[23] Kumar A, Vaity P and Singh R P 2011 Crafting the core asymmetry to lift the degeneracy of optical vortices *Opt. Express* **19** 6182–90